A Successive Parameter Estimation Algorithm for Chirplet Signal Decomposition

Yufeng Lu, *Student Member, IEEE*, Ramazan Demirli, *Member, IEEE*, Guilherme Cardoso, and Jafar Saniie, *Senior Member, IEEE*

***Abstract*—In ultrasonic imaging systems, the patterns of detected echoes correspond to the shape, size, and orientation of the reflectors and the physical properties of the propagation path. However, these echoes often are overlapped due to closely spaced reflectors and/or microstructure scattering. The decomposition of these echoes is a major and challenging problem. Therefore, signal modeling and parameter estimation of the nonstationary ultrasonic echoes is critical for image analysis, target detection, and object recognition. In this paper, a successive parameter estimation algorithm based on the chirplet transform is presented. The chirplet transform is used not only as a means for time-frequency representation, but also to estimate the echo parameters, including the amplitude, time-of-arrival, center frequency, bandwidth, phase, and chirp rate. Furthermore, noise performance analysis using the Cramer Rao lower bounds demonstrates that the parameter estimator based on the chirplet transform is a minimum variance and unbiased estimator for signal-to-noise ratio (SNR) as low as 2.5 dB. To demonstrate the superior time-frequency and parameter estimation performance of the chirplet decomposition, ultrasonic flaw echoes embedded in grain scattering, and multiple interfering chirplets emitted by a large, brown bat have been analyzed. It has been shown that the chirplet signal decomposition algorithm performs robustly, yields accurate echo estimation, and results in SNR enhancements. Numerical and analytical results show that the algorithm is efficient and successful in high-fidelity signal representation.**

I. Introduction

The chirp signal is a type of signal often encountered in ultrasound, radar, sonar, seismic signals, EEG and speech [1]–[13]. The chirp signal parameters represent valuable information pertaining to the shape, size and orientation of the reflectors in ultrasonic nondestructive evaluation, the location and velocity of the moving targets in radar-target detection, or the propagation path in seismic signal analysis. Recently, a modified, continuous wavelet transform (MCWT) based on the Gabor-Helstorm transformation has been introduced as a means to decompose ultrasonic echoes in terms of Gabor functions [14], [15]. The MCWT decomposition has not been found effective in representing ultrasonic echoes with chirp characteristics. Compared with the Gabor function [14], [15], the Gaussian chirplet model has one more parameter, the chirp rate, and thereby can better represent chirp-type signals. In this paper, we introduce a chirplet decomposition algorithm to represent chirp-type signals in terms of Gaussian chirplets, which are sparse and energy preserving. The sparseness property aims for a compact representation of the complex signal by decomposing it into a limited number of chirp components. The energy preservation property, by coherently distributing the signal energy into composing functions, enables the linear addition of the time-frequency (TF) distributions of composing functions to represent the TF of the signal. Hence, a high resolution TF representation can be achieved by decomposing the signal into a limited number of chirp functions with known TF distributions [16]–[18]. Furthermore, once the signal is decomposed by a family of chirplet echoes, these echoes, individually or collectively, can be used to describe the nonstationary behavior of the signal.

The chirplet signal decomposition (CSD) method uses the chirplet transform (CT) and a successive parameter estimation algorithm. Based on the CT of the signal, the algorithm identifies the location and duration of the most dominant chirp component in TF domain. Then, a successive parameter estimation algorithm is used to estimate the parameters of this dominant chirp component. The algorithm can recover the parameters of a noise-free chirp signal without requiring any initial guess for parameters. It accounts for a variety of differently shaped echoes, including narrow-band, broad-band, symmetric, skewed, dispersive, or nondispersive. Furthermore, the algorithm performs robustly in the presence of noise. Noise performance analysis using Cramer Rao lower bounds (CRLB) demonstrates that the parameter estimation is minimum variance and unbiased. The successive parameter estimation algorithm ensures the best representation of a chirp-type signal in terms of a Gaussian chirplet. Once a Gaussian chirplet is estimated, it is subtracted from the original signal, and the remaining signal is recursively decomposed into other Gaussian chirplets. The CSD algorithm has been tested on the simulated chirp-type ultrasonic echoes, experimental ultrasonic target echoes embedded in grain scattering, and multiple interfering chirplets emitted by a large, brown bat. In our study, the results demonstrate that the CSD algorithm achieves a high resolution TF representation and accurate parameter estimations. This type of study addresses a broad range of applications such as target detection, data compression, deconvolution, object classification, velocity measurement, and ranging systems.

In Section II, the chirplet transform and the mathematical description of the successive parameter estimation

Manuscript received November 8, 2005; accepted May 31, 2006.

The authors are with the Department of Electrical and Computer Engineering, Illinois Institute of Technology, Chicago, IL 60616 (e-mail: sansonic@ece.iit.edu).

Digital Object Identifier 10.1109/TUFFC.2006.152

algorithm based on the chirplet transform are discussed. Section III presents the performance analysis of estimation with noise using CRLB bounds and Monte-Carlo simulations. Section IV addresses the decomposition of complex chirp signals in terms of Gaussian chirps using an echo windowing method for successive parameter estimation. In Section V, the experimental data, including the ultrasonic backscattered signal, and bat chirp signal are evaluated using the CSD method.

II. CSD and Successive Parameter Estimation Algorithm

The objective of the successive parameter estimation algorithm is to efficiently estimate the parameters of the individual chirp echoes. The parameters can be used not only to reconstruct the original data but also as a quantitative procedure to examine the physical properties of the objects. In most application cases, a single chirp echo can be modeled as:

$$f_\Theta(t) = \beta \exp\big(-\alpha_1(t-\tau)^2 + i2\pi f_c(t-\tau) + i\phi + i\alpha_2(t-\tau)^2\big), \quad (1)$$

where $\Theta = [\alpha_1, \alpha_2, \beta, f_c, \phi, \tau]$ denotes the parameter vector, α_1 is the bandwidth factor, α_2 is the chirp-rate, β is the amplitude, f_c is the center frequency, ϕ is the phase, and τ is the time of arrival of the chirp echo. These parameters can be estimated successively using the CT. The successive parameter estimation algorithm is a recursive method that starts with the CT of the signal $f_\Theta(t)$. The CT of $f_\Theta(t)$ with respect to a chirplet kernel $\Psi_{\widehat{\Theta}}(t)$ is a TF representation and defined as:

$$CT\left(\widehat{\Theta}\right) = \int_{-\infty}^{+\infty} f_\Theta(t)\Psi^*_{\widehat{\Theta}}(t)dt, \quad (2)$$

where $\widehat{\Theta} = \left[\gamma_1, \gamma_2, \eta, \frac{\omega_0}{2\pi a}, \theta, b\right]$ denotes the parameter vector, $\Psi^*_{\widehat{\Theta}}(t)$ denotes the conjugate of chirplet kernel $\Psi_{\widehat{\Theta}}(t)$. The $\Psi_{\widehat{\Theta}}(t)$ is defined as:

$$\Psi_{\widehat{\Theta}}(t) = \eta \exp\Big(-\gamma_1(t-b)^2 + i\omega_0\left(\frac{t-b}{a}\right) + i\theta + i\gamma_2(t-b)^2\Big). \quad (3)$$

In order to normalize the energy of the chirplet kernel, the term $\eta = \left(\frac{2\gamma_1}{\pi}\right)^{\frac{1}{4}}$ is used. Hence, the CT of $f_\Theta(t)$ given by (1) can be expressed as:

$$CT\left(\widehat{\Theta}\right) = \beta\left(2\pi\gamma_1\right)^{\frac{1}{4}} \frac{1}{\sqrt{\alpha_1+\gamma_1-i\alpha_2+i\gamma_2}} \exp\left[-\frac{\left(\omega_c-\frac{\omega_0}{a}\right)^2}{4\left(\alpha_1+\gamma_1-i\alpha_2+i\gamma_2\right)} + i(\phi-\theta) - \frac{\left(\alpha_1-i\alpha_2\right)\left(\gamma_1+i\gamma_2\right)(b-\tau)^2}{\alpha_1+\gamma_1-i\alpha_2+i\gamma_2} + \frac{\left(i\frac{\omega_0}{a}\left(\alpha_1-i\alpha_2\right)+i\omega_c\left(\gamma_1+i\gamma_2\right)\right)(b-\tau)}{\alpha_1+\gamma_1-i\alpha_2+i\gamma_2}\right], \quad (4)$$

where $\omega_c = 2\pi f_c$. The maximum similarity between the input signal, $f_\Theta(t)$, and the chirplet kernel, $\Psi_\Theta(t)$, leads to correct estimation of echo parameters, $\widehat{\Theta}$. The peak of $CT(\widehat{\Theta})$ can be used to estimate the center frequency, f_c, and time of arrival, τ. To accomplish this goal, the magnitude of the $CT(\widehat{\Theta})$ is used for estimation of the signal parameters, which is given by:

$$\left|CT\left(\widehat{\Theta}\right)\right| = \beta\left(2\pi\gamma_1\right)^{\frac{1}{4}}\left[\left(\alpha_1+\gamma_1\right)^2+\left(\alpha_2-\gamma_2\right)^2\right]^{-\frac{1}{4}} \exp\left[-\frac{\left(\omega_c-\frac{\omega_0}{a}\right)^2\left(\alpha_1+\gamma_1\right)^2}{4\left(\left(\alpha_1+\gamma_1\right)^2+\left(\alpha_2-\gamma_2\right)^2\right)} - \frac{\left(\omega_c-\frac{\omega_0}{a}\right)\left(\alpha_1\gamma_2+\alpha_2\gamma_1\right)(b-\tau)}{\left(\alpha_1+\gamma_1\right)^2+\left(\alpha_2-\gamma_2\right)^2} - \frac{\left(\alpha_1^2\gamma_1+\alpha_2^2\gamma_1+\gamma_1^2\alpha_1+\gamma_2^2\alpha_1\right)(b-\tau)^2}{\left(\alpha_1+\gamma_1\right)^2+\left(\alpha_2-\gamma_2\right)^2}\right]. \quad (5)$$

The maximum of (5) can be obtained by taking partial derivatives of $\left|CT\left(\widehat{\Theta}\right)\right|$ with respect to a (which corresponds to the center frequency, f_c) and b (which corresponds to the time of arrival, τ):

$$\frac{\partial\left|CT\left(\widehat{\Theta}\right)\right|}{\partial a} = \left|CT\left(\widehat{\Theta}\right)\right|\left\{\frac{-\omega_0 a^{-2}\left(\alpha_1\gamma_2+\alpha_2\gamma_1\right)(b-\tau)}{2\left(\left(\alpha_1+\gamma_1\right)^2+\left(\alpha_2-\gamma_2\right)^2\right)} + \frac{\frac{\omega_0}{a^2}\left(\frac{\omega_0}{a}-\omega_c\right)\left(\alpha_1+\gamma_1\right)}{2\left(\left(\alpha_1+\gamma_1\right)^2+\left(\alpha_2-\gamma_2\right)^2\right)}\right\} = 0, \quad (6)$$

$$\frac{\partial\left|CT\left(\widehat{\Theta}\right)\right|}{\partial b} = \left|CT\left(\widehat{\Theta}\right)\right|\left\{\frac{-\left(\alpha_1^2\gamma_1+\alpha_2^2\gamma_1+\alpha_1\gamma_1^2+\alpha_1\gamma_2^2\right)(b-\tau)}{2\left(\left(\alpha_1+\gamma_1\right)^2+\left(\alpha_2-\gamma_2\right)^2\right)} + \frac{\left(\frac{\omega_0}{a}-\omega_c\right)\left(\alpha_1\gamma_2+\alpha_2\gamma_1\right)}{4\left(\left(\alpha_1+\gamma_1\right)^2+\left(\alpha_2-\gamma_2\right)^2\right)}\right\} = 0. \quad (7)$$

The solutions of (6) and (7) lead to an estimation of center frequency and time of arrival:

$$b = \tau, \quad \frac{\omega_0}{a} = \omega_c. \quad (8)$$

In (8) the estimation of the peak position of $\left|CT\left(\widehat{\Theta}\right)\right|$ is not a function of the bandwidth factor, γ_1, chirp-rate, γ_2, and phase, θ, of the echo. Furthermore, the peak value of $\left|CT\left(\widehat{\Theta}\right)\right|$ is proportional to the amplitude of the actual echo and leads to the estimation of β.

Based on the above estimations of a and b, the estimation of the chirp-rate, γ_2 becomes a one-dimensional estimation problem. This can be achieved by taking the

derivative of $\left|CT\left(\widehat{\Theta}\right)\right|$ with respect to γ_2 and setting it to 0:

$$\frac{\partial\left|CT\left(\widehat{\Theta}\right)\right|}{\partial\gamma_2}=\left|CT\left(\widehat{\Theta}\right)\right|\left[\frac{\alpha_2-\gamma_2}{2\left(\left(\alpha_1+\gamma_1\right)^2+\left(\alpha_2-\gamma_2\right)^2\right)}-\frac{\alpha_1\left(\omega_c-\frac{\omega_0}{a}\right)(b-\tau)+2\gamma_2\alpha_1(b-\tau)^2}{\left(\alpha_1+\gamma_1\right)^2+\left(\alpha_2-\gamma_2\right)^2}-\frac{\left(\alpha_2-\gamma_2\right)\left(\omega_c-\frac{\omega_0}{a}\right)^2\left(\alpha_1+\gamma_1\right)^2}{2\left(\left(\alpha_1+\gamma_1\right)^2+\left(\alpha_2-\gamma_2\right)^2\right)^2}-\frac{2\left(\alpha_2-\gamma_2\right)\left(\omega_c-\frac{\omega_0}{a}\right)\left(\alpha_1\gamma_2+\alpha_2\gamma_1\right)(b-\tau)}{\left(\left(\alpha_1+\gamma_1\right)^2+\left(\alpha_2-\gamma_2\right)^2\right)^2}-\frac{2\left(\alpha_2-\gamma_2\right)\left(\alpha_1^2\gamma_1+\alpha_2^2\gamma_1+\gamma_1^2\alpha_1+\gamma_2^2\alpha_1\right)(b-\tau)^2}{\left(\left(\alpha_1+\gamma_1\right)^2+\left(\alpha_2-\gamma_2\right)^2\right)^2}\right]. \quad (9)$$

Hence, the maximum of $\left|CT\left(\widehat{\Theta}\right)\right|$ yields the optimal solution of γ_2:

$$\left.\frac{\partial\left|CT\left(\widehat{\Theta}\right)\right|}{\partial\gamma_2}\right|_{b=\tau,\frac{\omega_0}{a}=\omega_c}=\frac{2\left(\alpha_2-\gamma_2\right)}{\left(\alpha_1+\gamma_1\right)^2+\left(\alpha_2-\gamma_2\right)^2}\left|CT\left(\widehat{\Theta}\right)\right|_{b=\tau,\frac{\omega_0}{a}=\omega_c}=0. \quad (10)$$

The solution to (10) is:

$$\gamma_2=\alpha_2. \quad (11)$$

Similarly, the estimation of the bandwidth factor, γ_1, is carried out by taking the partial derivative of $\left|CT\left(\widehat{\Theta}\right)\right|$ in respect to γ_1, and setting it to 0:

$$\frac{\partial\left|CT\left(\widehat{\Theta}\right)\right|}{\partial\gamma_1}=\left|CT\left(\widehat{\Theta}\right)\right|\left[\frac{\left(\alpha_1^2-\gamma_1^2\right)+\left(\alpha_2-\gamma_2\right)^2}{4\gamma_1\left(\left(\alpha_1+\gamma_1\right)^2+\left(\alpha_2-\gamma_2\right)^2\right)}-\frac{\left(\omega_c-\frac{\omega_0}{a}\right)^2\left(\alpha_1+\gamma_1\right)}{2\left(\left(\alpha_1+\gamma_1\right)^2+\left(\alpha_2-\gamma_2\right)^2\right)^2}-\frac{\alpha_2\left(\omega_c-\frac{\omega_0}{a}\right)(b-\tau)+\left(\alpha_1^2+\alpha_2^2\right)(b-\tau)^2}{\left(\alpha_1+\gamma_1\right)^2+\left(\alpha_2-\gamma_2\right)^2}-\frac{\left(\omega_c-\frac{\omega_0}{a}\right)^2\left(\alpha_1+\gamma_1\right)^3}{2\left(\left(\alpha_1+\gamma_1\right)^2+\left(\alpha_2-\gamma_2\right)^2\right)^2}-\frac{2\left(\alpha_1+\gamma_1\right)\left(\omega_c-\frac{\omega_0}{a}\right)\left(\alpha_1\gamma_2+\alpha_2\gamma_1\right)(b-\tau)}{\left(\left(\alpha_1+\gamma_1\right)^2+\left(\alpha_2-\gamma_2\right)^2\right)^2}-\frac{2\left(\alpha_1+\gamma_1\right)\left(\alpha_1^2\gamma_1+\alpha_2^2\gamma_1+\gamma_1^2\alpha_1+\gamma_2^2\alpha_1\right)(b-\tau)^2}{\left(\left(\alpha_1+\gamma_1\right)^2+\left(\alpha_2-\gamma_2\right)^2\right)^2}\right]. \quad (12)$$

Hence:

$$\left.\frac{\partial\left|CT\left(\widehat{\Theta}\right)\right|}{\partial\gamma_1}\right|_{\substack{b=\tau,\\ \frac{\omega_0}{a}=\omega_c,\\ \gamma_2=\alpha_2}}=\left(\frac{\alpha_1^2-\gamma_1^2}{4\gamma_1\left(\alpha_1+\gamma_1\right)^2}\right)\left|CT\left(\widehat{\Theta}\right)\right|_{\substack{b=\tau,\\ \frac{\omega_0}{a}=\omega_c,\\ \gamma_2=\alpha_2}}=0. \quad (13)$$

The solution to (13) yields:

$$\gamma_1=\alpha_1. \quad (14)$$

Because there is no information about signal phase in the magnitude representation of the CT, the real part of the CT is used to estimate the phase of the echo, θ.

$$\mathrm{Re}\left(CT\left(\widehat{\Theta}\right)\right)=\left|CT\left(\widehat{\Theta}\right)\right|\cos\left[\left(\frac{1}{2}\tan^{-1}\frac{\alpha_2-\gamma_2}{\alpha_1+\gamma_1}\right)+(\varphi-\theta)-\frac{\left(\omega_c-\frac{\omega_0}{a}\right)^2\left(\alpha_2-\gamma_2\right)}{4\left(\left(\alpha_1+\gamma_1\right)^2+\left(\alpha_2-\gamma_2\right)^2\right)}+\frac{\alpha_2\left(\gamma_1^2+\gamma_2^2\right)-\left(\alpha_1^2+\alpha_2^2\right)\gamma_2}{\left(\alpha_1+\gamma_1\right)^2+\left(\alpha_2-\gamma_2\right)^2}(b-\tau)^2+\frac{\omega_c\left(\gamma_1^2+\gamma_2^2\right)-\left(\alpha_1^2+\alpha_2^2\right)\frac{\omega_0}{a}}{\left(\alpha_1+\gamma_1\right)^2+\left(\alpha_2-\gamma_2\right)^2}(b-\tau)+\frac{\left(\omega_c+\frac{\omega_0}{a}\right)\left(\alpha_1\gamma_1-\alpha_2\gamma_2\right)}{\left(\alpha_1+\gamma_1\right)^2+\left(\alpha_2-\gamma_2\right)^2}(b-\tau)\right]. \quad (15)$$

Based on the above estimations of a, b, and γ_2, the estimation of phase, θ, becomes a one-dimensional estimation problem. The maximum of $\mathrm{Re}\left(CT\left(\widehat{\Theta}\right)\right)$ yields the optimal solution for θ. This can be obtained by taking the partial derivative of $\mathrm{Re}\left(CT\left(\widehat{\Theta}\right)\right)$ with respect to θ and setting it to 0:

$$\left.\frac{\partial\,\mathrm{Re}\left(CT\left(\widehat{\Theta}\right)\right)}{\partial\theta}\right|_{\substack{b=\tau,\frac{\omega_0}{a}=\omega_c,\\ \gamma_2=\alpha_2}}=\sin(\theta-\phi)\,\mathrm{Re}\left(CT\left(\widehat{\Theta}\right)\right)\Big|_{\substack{b=\tau,\frac{\omega_0}{a}=\omega_c,\\ \gamma_2=\alpha_2}}=0. \quad (16)$$

The solution of (16) yields:

$$\theta=\phi\pm 2k\pi,\quad k=1,2,3,\ldots \quad (17)$$

In summary, the mathematical steps presented above show that the chirplet transform leads to an exact estimation of the time of arrival, center frequency, phase, bandwidth factor, and chirp rate of the chirp-echo signal. The parameter estimations based on these equations can be implemented successively using signal correlation (2). A grid search is performed to find the value of the parameter that maximizes the signal correlation. Furthermore, the estimations of these parameters are refined with a fast Gauss-Newton algorithm [16]–[18]. The refinement improves the

TABLE I
COMPARISON OF THE CRLB'S WITH THE VARIANCES OF ESTIMATORS FOR DIFFERENT SNR.

	α_1 [MHz]^2	α_2 [MHz]^2	τ [μs]	f_c [MHz]	ϕ [rad]	β
Actual Parameter	25	15	1	5	1	1
20.00 dB SNR						
Mean	25.0266	15.0080	0.9999	4.9996	0.9959	1.0007
Variance	4.4831e-1	5.6883e-1	4.5664e-6	3.4852e-4	4.5799e-3	1.5671e-4
CRLB	5.0000e-1	5.0000e-1	4.0000e-6	3.4449e-4	4.0978e-3	1.5000e-4
15.00 dB SNR						
Mean	24.9987	15.0932	0.9997	4.9998	0.9906	0.9999
Variance	1.5547	1.3617	1.2474e-5	1.2403e-3	1.3101e-2	4.8127e-4
CRLB	1.5811	1.5811	1.2649e-5	1.1000e-3	1.3000e-2	4.7434e-4
10.00 dB SNR						
Mean	25.0242	14.8368	0.9997	4.9967	0.9911	1.0011
Variance	4.0620	5.4588	3.5395e-5	3.4286e-3	3.4439e-2	1.4117e-3
CRLB	5.0000	5.0000	4.0000E-5	3.4000e-3	4.1000e-2	1.5000e-3
5.00 dB SNR						
Mean	24.7932	15.2223	0.9997	4.9933	0.9905	1.0080
Variance	14.4450	16.9490	1.3875e-4	1.1230e-2	1.4020e-1	3.8953e-3
CRLB	15.8114	15.8114	1.0000e-4	1.0900e-2	1.2960e-1	4.7000e-3
2.50 dB SNR						
Mean	24.9589	15.0622	0.9981	4.9912	0.8623	1.0152
Variance	33.4220	33.3590	2.1771e-4	2.0220e-2	6.2925e-1	9.6703e-3
CRLB	28.1171	28.1171	2.0000e-4	1.9400e-2	2.3040e-1	8.4000e-3

parameter estimation beyond the resolution of the search grid. The successive parameter estimation based on the CSD method can recover the exact value of the parameters of a noise-free Gaussian chirp echo. It does not require any initial guess for the parameters before estimation. Furthermore, it also can estimate the parameters of a noise corrupted echo with high accuracy. In the next section we analyze the performance of estimation with noise using CRLB.

III. Performance Analysis Using CRLB

In order to evaluate the performance of estimation in the presence of noise, we consider a single chirp echo in white Gaussian noise with varying noise levels, and we observe the bias and variation in the parameter estimation. Specifically, we use the following observed chirp model:

$$r(t;\Theta) = s(t;\Theta) + n(t), \tag{18}$$

where $s(t;\Theta)$ represents the chirp echo and $n(t)$ represents the zero-mean white Gaussian noise with variance σ^2. The CRLB for the parameter vector Θ can be analytically computed using:

$$\text{Var}\left(\widehat{\Theta}\right) \geq \left[I^{-1}(\Theta)\right], \tag{19}$$

where $I(\Theta)$ is the Fisher information matrix (FIM). For the above observed signal model $r(t;\Theta)$ is normally distributed as $N\left(s(t;\Theta), \sigma^2 I\right)$. Hence, the FIM can be written as [19]:

$$I(\Theta) = \frac{H^T(\Theta)H(\Theta)}{\sigma^2}, \tag{20}$$

where $H(\Theta)$ represents the gradients of the chirp echo model. The analytical derivation of the gradients, FIM and the CRLB, are given in the Appendix, which yields the variance bounds of the estimated chirplet parameters under noise are:

$$\begin{aligned}
\text{Var}\left(\hat{\alpha}_1\right) &\geq \frac{8\alpha_1^2}{f_s\zeta},\\
\text{Var}\left(\hat{\alpha}_2\right) &\geq \frac{8\alpha_1^2}{f_s\zeta},\\
\text{Var}\left(\hat{\tau}\right) &\geq \frac{1}{\alpha_1 f_s\zeta},\\
\text{Var}\left(\hat{f}_c\right) &\geq \frac{\alpha_1^2+\alpha_2^2}{\pi^2\alpha_1 f_s\zeta},\\
\text{Var}\left(\hat{\phi}\right) &\geq \frac{\frac{3}{2}+\frac{(2\pi f_c)^2}{\alpha_1}}{f_s\zeta},\\
\text{Var}\left(\hat{\beta}\right) &\geq \frac{3\beta^2}{2f_s\zeta},
\end{aligned} \tag{21}$$

where f_s denotes sampling rate and ζ denotes SNR.

To evaluate the performance of estimation, a Monte-Carlo simulation is performed to observe the means and variances of the estimated parameters of a single noisy echo given in (18). The chirp echo is simulated according to (1) with the parameter vector listed in the first row of Table I. The sampling frequency is 100 MHz. The noise level is adjusted to simulate echoes with SNR levels of 20, 15, 10, 5, and 2.5 dB. For each SNR level, the parameter estimation is performed 250 times on the simulated chirp echo with different realizations of noise. The average value and the variance of parameter estimators are listed in Table I along with the analytically computed CRLB's using

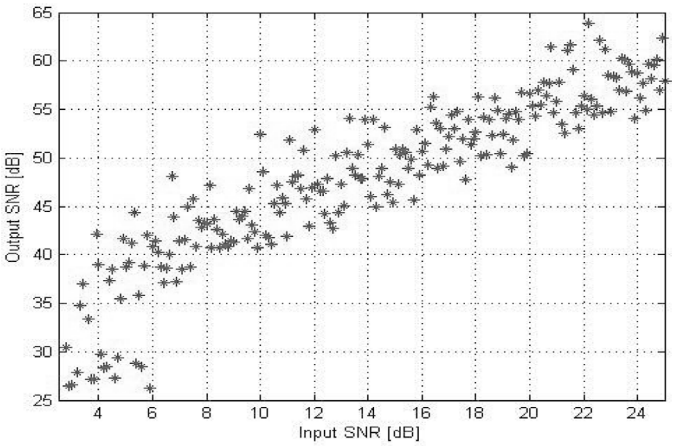

Fig. 1. Input SNR versus output SNR for a single noisy chirp echo.

(21). One can observe that the parameter estimation is unbiased, i.e., the mean value of the estimated parameters achieves the actual parameter values used in simulation, and the variance of estimators attains the CRLB bounds for SNR as low as 2.5 dB. Therefore, the successive parameter estimation based on the CSD method is a minimum variance unbiased (MVU) estimator for a single chirp echo and, hence, provides optimal parameter estimation results.

The parameter estimation algorithm significantly improves the SNR of chirp signals. To quantify the SNR improvement, a chirp echo with varying noise level is simulated. After estimation is performed, the output SNR (i.e., an estimated SNR) is computed as the energy ratio of the original signal and residual error, i.e., the difference between the original and the estimated signal. Fig. 1 shows the output SNR as a function of the input SNR. Each point in this plot represents a realization of the signal with a different noise level. The parameters of the single echo have not been changed. The input SNR has been varied from 2.5 dB (severely poor SNR) to 25 dB (high SNR). It has been observed that the average SNR enhancement for the single echo in white Gaussian noise is well above 20 dB. It is important to point out that one should expect a smaller SNR enhancement when the signal contains overlapping chirp echoes and is corrupted by correlated noise.

IV. Chirplet Signal Decomposition

We use the successive parameter estimation technique to decompose a complex signal into a small number of Gaussian chirplets. The complex signal will be represented by the linear addition of a number of chirplets:

$$s(t) = \sum_{j=0}^{N-1} f_{\Theta_j}(t), \tag{22}$$

where $f_{\Theta_j}(t)$ is the chirplet model and Θ_j is the parameter vector of $f_{\Theta_j}(t)$, see (1).

The goal of signal decomposition is to express the signal $s(t)$ as a linear combination of chirp components. The decomposition is performed as follows. First, based on the CT of the signal (i.e., TF representation), the most dominant chirp echo is windowed and estimated using the successive parameter estimation algorithm presented in Section II. Second, the estimated echo is subtracted from the original signal. Third, the second echo is estimated from the remaining signal. This process is repeated until the reconstruction error, E_r, is below an acceptable value E_{min}. The value of E_{min} is determined based on the requirements of the reconstruction quality of the signal. This iterative decomposition method ensures energy preservation by coherently distributing the signal energy into composing functions. Energy preservation allows us to add the TF distribution of composing functions $f_{\Theta_j}(t)$ to estimate the TF distribution of the signal $s(t)$. Meanwhile, the sparseness of decomposition is ensured by searching for the most dominant chirp echo per iteration. A block diagram summarizing the CSD algorithm is shown in Fig. 2.

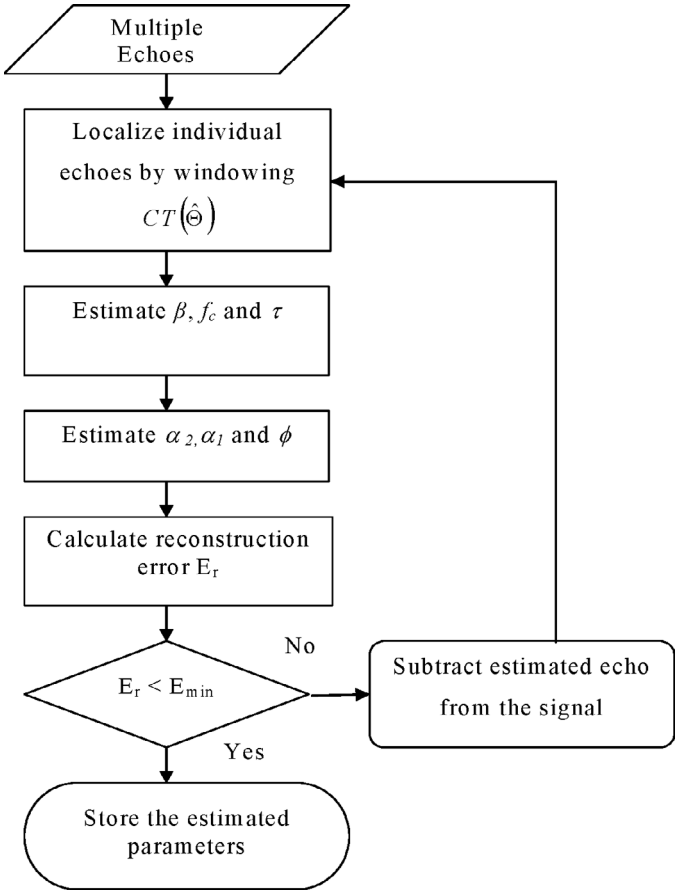

Fig. 2. The flowchart of the CSD algorithm.

The procedure used to design the window is based on the determination of the peaks and valleys of the CT of the signal. Fig. 3 illustrates the windowing method with simulated data containing three interfering echoes. First, the maximum peak of the CT of the signal [Fig. 3(a)] is identified. Second, the CT of the signal is projected onto the time domain [Fig. 3(c)] and frequency domain [Fig. 3(b)]. The windowing algorithm uses these projections to isolate the dominant echo by tracing the nearest valleys around the

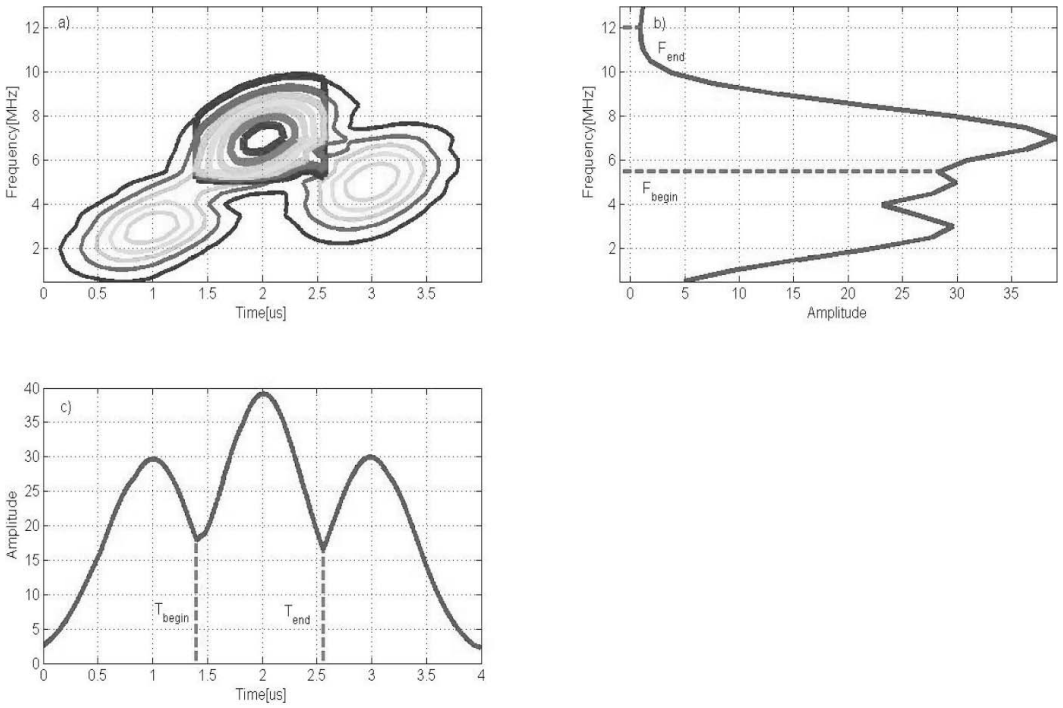

Fig. 3. Basic illustration of dominant echo windowing method: (a) CT of three interfering chirp echoes. The most dominant echo is emphasized after time and frequency windowing. (b) Projection in frequency domain and the frequency-window boundary points (dashed lines). (c) Projection in time domain and the time-window boundary points (dashed lines).

peak. The closest two valleys confining the time-projection peak are defined as the boundaries of the time-window [i.e., T_{begin} and T_{end} in Fig. 3(c)]. Similarly, the closest two valleys confining the frequency projection peak are defined as the boundaries of the frequency window [i.e., F_{begin} and F_{end} in Fig. 3(b)]. The time of arrival τ and center frequency f_c parameters are in fact the peak locations of the projections (8). The dominant signal along with the time window and frequency window is used to estimate the remaining chirplet parameters (i.e., amplitude β, bandwidth γ_1, chirp rate γ_2, and phase θ) using signal correlation (see Section II).

When there are heavily overlapping echoes and high noise levels, the performance of the automatic windowing method may be compromised as the peak separation process becomes more difficult. The distance between peaks becomes shorter, and artificial valley points may be created due to the noise. In these cases, a time window and frequency window with predetermined size can be used to separate out the time and frequency projection peaks. The windows are centered at the peaks. The sizes of the windows can be determined by inspecting the CT of the measured signal for given noise levels. A good window size selection strategy is to keep as much of the signal energy as possible while suppressing the contribution of noise energy in the window. For the simulated and experimental signals presented in this study, the automatic windowing method performed adequately in extracting the individual echoes. However, one can apply the predetermined windowing method for signals with very poor SNRs (2 dB and below).

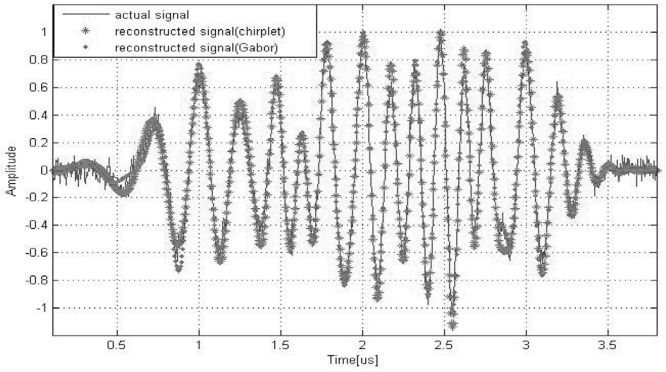

Fig. 4. Simulated ultrasonic highly overlapping chirplets (solid line), superimposed with the reconstructed signals by the CSD method and Gabor decomposition method.

The CSD algorithm is very effective in representing dispersive ultrasonic echoes. An alternative decomposition algorithm [14] uses a Gabor kernel to analyze ultrasonic echoes. However, if the ultrasonic signal has a dispersive or frequency shift property, Gabor decomposition requires many components. The chirplet model is expected to have better decomposition efficiency with extra parameter diversity. To demonstrate chirplet decomposition efficiency, a noisy chirp signal containing highly overlapping echoes is simulated, then the algorithm presented in [14] and the CSD algorithm are both applied to reconstruct the signal. Fig. 4 shows the noisy chirp signal and the two reconstruction results from these two different decomposition strategies, under the same output SNR criteria. More specifically, the parameters of the decomposed echoes are listed

TABLE II
PARAMETERS OF DECOMPOSED ECHOES (GABOR DECOMPOSITION METHOD [14]).

Echo no.	α_1 [MHz]^2	τ [μs]	f_c [MHz]	ϕ [rad]	β
1	19.70	1.91	4.86	3.91	1.01
2	16.18	2.54	6.92	9.09	0.97
3	27.00	3.02	4.65	0.73	0.88
4	7.13	1.10	4.06	2.69	0.65
5	41.11	2.69	3.95	5.67	0.39
6	3.44	1.97	7.31	−2.57	0.34
7	65.66	3.31	5.73	4.47	0.27
8	36.10	1.58	3.66	−2.85	0.26
9	4.22	0.86	2.68	−3.10	0.23
10	1.84	1.82	5.87	6.63	0.18
11	10.08	2.72	8.82	−1.84	0.11

TABLE III
PARAMETERS OF DECOMPOSED ECHOES (CSD METHOD).

Echo no.	α_1 [MHz]^2	α_2 [MHz]^2	τ [μs]	f_c [MHz]	ϕ [rad]	β
1	16.86	7.53	2.54	6.86	8.88	0.99
2	13.13	16.71	1.97	5.04	5.24	0.96
3	11.73	16.82	3.00	4.51	0.02	0.78
4	4.36	8.44	1.09	3.95	2.07	0.64
5	6.28	4.32	1.67	6.89	1.95	0.34

in Table II and Table III. It can be seen that, the chirplet decomposition algorithm requires a significantly less number of components than Gabor decomposition [14]. The compact representation achieved by the chirplet decomposition is more powerful in revealing the physical properties of chirp-type signals (e.g., the Doppler shift in a radar system, the dispersive echoes in an ultrasonic nondestructive testing system).

V. CHIRPLET DECOMPOSITION OF EXPERIMENTAL DATA

The CSD algorithm is evaluated using an ultrasonic experimental signal consisting of many interfering echoes. Fig. 5 shows an experimental signal acquired from a steel block with a flat-bottom hole (i.e., target) using a 5 MHz transducer and sampling rate of 100 MHz. The experimental signal has poor SNR, and the target echo shows interference from microstructure scattering and measurement noise. The reconstructed signal and its CT representation are shown in Fig. 6(c) and (d). The comparison between the experimental signal and the reconstructed signal (see Figs. 5 and 6) clearly demonstrates that the chirplet signal decomposition has been successful in estimating echoes and filtering out the noise.

Furthermore, the CSD algorithm is applied to a bat chirp signal emitted by the large, brown bat [20], which is

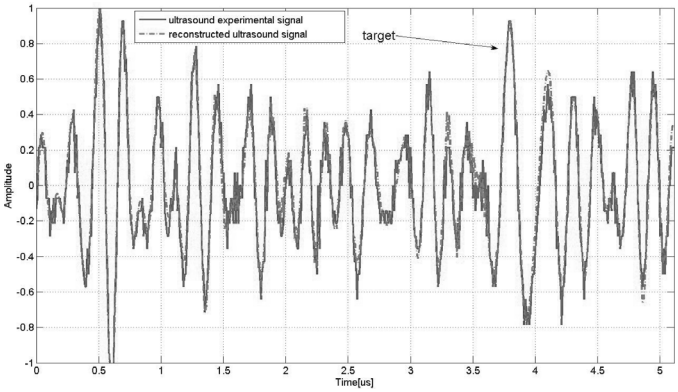

Fig. 5. Measured ultrasonic backscattered signal superimposed with reconstructed signal.

digitized within 2.2 ms duration with a 7 μs sampling period. It can be seen that, from Fig. 7 and Fig. 8(a) and (b), the bat signal is a complex chirp with poor SNR and contains heavily overlapping, chirp components not only in the time domain but also in the frequency domain. Fig. 8(c) and (d) show the reconstructed signal and its CT using 15 individual chirplet echoes.

VI. CONCLUSIONS

In this study, we analyzed a CSD modeling and successive parameter estimation algorithm to decompose ultrasonic signals with multiple interfering echoes into Gaussian chirplets. A successive parameter estimation algorithm based on CT and an automatic echo windowing method have been developed to estimate the time of arrival, the center frequency, the phase, the bandwidth, the chirp rate, and the amplitude of chirp echoes. Monte-Carlo simulation results demonstrate that the successive parameter estimation is unbiased and exhibit minimum variance, i.e., the variances in the parameter estimators attain the CRLB. The CSD is sparse and energy preserving; hence, it provides a high resolution and compact TF representation of the signal. It has been shown through computer simulation and analysis of experimental data that the chirplet decomposition algorithm can efficiently decompose the chirp-type signals into Gaussian chirplets. The signal modeling and parameter estimation algorithm presented in this paper not only offers a signal decomposition method, but also provides parameters that can be used for data compression, pattern recognition, signal deconvolution, target detection, object sizing, and material characterization.

APPENDIX A
ANALYTICAL DERIVATIONS OF CRLB BOUNDS

The Gaussian chirplet echo is defined by the following model:

$$s(t;\Theta) = \beta e^{-\alpha_1 (t-\tau)^2} \cos\left[\alpha_2 (t-\tau)^2 + 2\pi f_c (t-\tau) + \phi\right], \quad \text{(A1)}$$

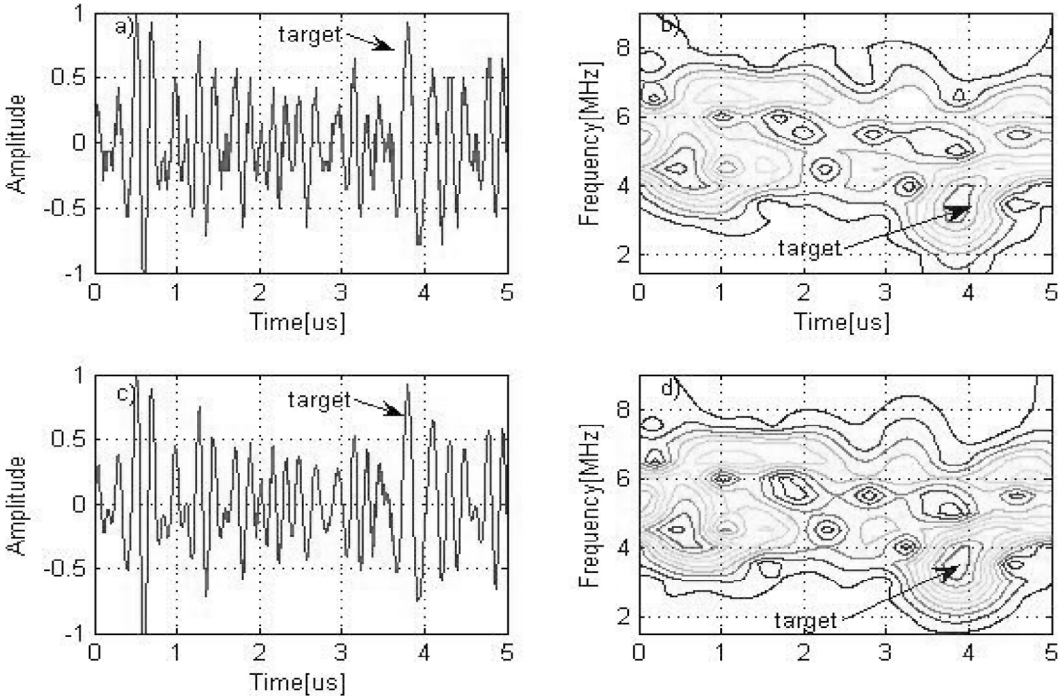

Fig. 6. (a) Ultrasonic backscattered signal. (b) CT of ultrasonic backscattering signal in (a). (c) Reconstructed signal. (d) CT of the reconstructed signal in (c).

where $\Theta = [\alpha_1\ \alpha_2\ \tau\ f_c\ \phi\ \beta]$ denotes the parameter vector. To simplify analytical derivations, consider the following kernel functions:

$$f(t;\Theta) = e^{-\alpha_1(t-\tau)^2}\cos\left[\alpha_2(t-\tau)^2 + 2\pi f_c(t-\tau) + \phi\right],$$
$$g(t;\Theta) = e^{-\alpha_1(t-\tau)^2}\sin\left[\alpha_2(t-\tau)^2 + 2\pi f_c(t-\tau) + \phi\right]. \tag{A2}$$

The partial derivatives of the chirplet with respect to parameters can be written in terms of the kernel functions:

$$\begin{aligned}
\frac{\partial s(t;\Theta)}{\partial \alpha_1} &= -\beta(t-\tau)^2 f(t;\Theta),\\
\frac{\partial s(t;\Theta)}{\partial \alpha_2} &= -\beta(t-\tau)^2 g(t;\Theta),\\
\frac{\partial s(t;\Theta)}{\partial \tau} &= 2\alpha_1\beta(t-\tau)f(t;\Theta) + \beta g(t;\Theta)\left[2\pi f_c + 2\alpha_2(t-\tau)\right],\\
\frac{\partial s(t;\Theta)}{\partial f_c} &= -2\pi\beta(t-\tau)g(t;\Theta),\\
\frac{\partial s(t;\Theta)}{\partial \phi} &= -\beta g(t;\Theta),\\
\frac{\partial s(t;\Theta)}{\partial \beta} &= f(t;\Theta).
\end{aligned} \tag{A3}$$

The FIM for a parametric signal in zero-mean white Gaussian noise (WGN) is defined as [19]:

$$I(\Theta) = \frac{H^T(\Theta)H(\Theta)}{\sigma^2}, \tag{A4}$$

where σ^2 denotes the noise variance (i.e., noise energy) and $H(\Theta)$ denotes the gradient matrix. $H(\Theta)$ can be written in terms of the partial derivatives (A3):

$$H(\Theta) = \left[\frac{\partial \overline{s}}{\partial\alpha_1}\ \frac{\partial \overline{s}}{\partial\alpha_2}\ \frac{\partial \overline{s}}{\partial\tau}\ \frac{\partial \overline{s}}{\partial f_c}\ \frac{\partial \overline{s}}{\partial\phi}\ \frac{\partial \overline{s}}{\partial\beta}\right], \tag{A5}$$

where $\overline{s}$ denotes the discrete signal obtained by sampling $s(t;\Theta)$ with sampling frequency f_s. Each element of the matrix $H^T(\Theta)H(\Theta)$ can be computed explicitly using the following approximation (see Appendix of [16]):

$$\begin{aligned}
\left[H^T(\Theta)H(\Theta)\right]_{ij} &= \left[\frac{\partial \overline{s}}{\partial\Theta_i}\right]^T\left[\frac{\partial \overline{s}}{\partial\Theta_j}\right]\\
&\cong f_s\int_{-\infty}^{\infty}\frac{\partial s(t;\Theta)}{\partial\Theta_i}\cdot\frac{\partial s(t;\Theta)}{\partial\Theta_j}dt,
\end{aligned} \tag{A6}$$

where Θ_i denotes the i-th parameter in the parameter vector and $1 \le i \le 6$, $1 \le j \le 6$.

To simplify mathematical expressions, we define the following variables:

$$A_{ij} = \int_{-\infty}^{\infty}\frac{\partial s(t;\Theta)}{\partial\Theta_i}\cdot\frac{\partial s(t;\Theta)}{\partial\Theta_j}dt, \tag{A7}$$

$$E = \frac{\pi^{\frac{1}{2}}}{2^{\frac{3}{2}}\alpha_1^{\frac{1}{2}}}, \tag{A8}$$

$$F_{ijk} = \int_{-\infty}^{\infty}(t-\tau)^i f^j(t;\Theta)g^k(t;\Theta)dt. \tag{A9}$$

Hence, the computation of $H^T(\Theta)H(\Theta)$ reduces to the computation of the following expressions:

$$\begin{aligned}
A_{11} &= \beta^2 F_{420},\\
A_{12} &= \beta^2 F_{411},\\
A_{13} &= -2\alpha_1\beta^2 F_{320} - 2\pi f_c\beta^2 F_{211} - 2\alpha_2\beta^2 F_{311},\\
A_{14} &= 2\pi\beta^2 F_{311},\\
A_{15} &= \beta^2 F_{211},\\
A_{16} &= -\beta F_{220},\\
A_{22} &= \beta^2 F_{402},\\
A_{23} &= -2\alpha_1\beta^2 F_{311} - 2\pi f_c\beta^2 F_{202} - 2\alpha_2\beta^2 F_{302},\\
A_{24} &= 2\pi\beta^2 F_{302},\\
A_{25} &= \beta^2 F_{202},\\
A_{26} &= -\beta F_{211},\\
A_{33} &= (2\alpha_1\beta)^2 F_{220} + (2\pi f_c)^2\beta^2 F_{020} + 4\pi f_c\alpha_2\beta^2 F_{102}\\
&\quad + (2\alpha_2\beta)^2 F_{202} + 8\pi f_c\alpha_1\beta^2 F_{111} + 8\alpha_1\alpha_2\beta^2 F_{211},\\
A_{34} &= -4\pi\alpha_1\beta^2 F_{211} - 4\pi^2 f_c\beta^2 F_{102} - 4\pi\alpha_2\beta^2 F_{202},\\
A_{35} &= -2\alpha_1\beta^2 F_{111} - 2\pi f_c\beta^2 F_{002} - 2\alpha_2\beta^2 F_{102},\\
A_{36} &= 2\alpha_1\beta F_{120} + 2\pi f_c\beta F_{011} + 2\alpha_2\beta F_{111},\\
A_{44} &= (2\pi\beta)^2 F_{202},\\
A_{45} &= 2\pi\beta^2 F_{102},\\
A_{46} &= -2\pi\beta F_{111},\\
A_{55} &= \beta^2 F_{002},\\
A_{56} &= -\beta F_{011},\\
A_{66} &= F_{020}.
\end{aligned} \tag{A10}$$

All F_{ijk} $(0 \le i \le 4,\ 0 \le j \le 2,\ 0 \le k \le 2)$ can be computed in Fourier domain. Hence, the following results for F_{ijk} can be obtained:

$$\begin{aligned}
&F_{120} = F_{102} = F_{320} = F_{302} = 0,\\
&F_{111} = F_{211} = F_{311} = F_{411} = 0,\\
&F_{020} = F_{002} = E,\\
&F_{220} = F_{202} = \frac{1}{8\alpha_1}\sqrt{\frac{\pi}{2\alpha_1}} = \frac{1}{4\alpha_1}E,\\
&F_{420} = F_{402} = \frac{3}{32\alpha_1^2}\sqrt{\frac{\pi}{2\alpha_1}} = \frac{3}{16\alpha_1^2}E.
\end{aligned} \tag{A11}$$

Using all of the above expressions, the FIM can be computed as:

$$I(\Theta) = \frac{H^T(t;\Theta)H(t;\Theta)}{\sigma^2} = \frac{\beta^2 f_s E}{\sigma^2}$$
$$\times \begin{bmatrix}
\frac{3}{16\alpha_1^2} & 0 & 0 & 0 & 0 & -\frac{1}{4\alpha_1\beta}\\
0 & \frac{3}{16\alpha_1^2} & \frac{-2\pi f_c}{4\alpha_1} & 0 & \frac{1}{4\alpha_1} & 0\\
0 & \frac{-2\pi f_c}{4\alpha_1} & \frac{\alpha_1^2+\alpha_2^2}{\alpha_1} + (2\pi f_c)^2 & \frac{-\pi\alpha_2}{\alpha_1} & -2\pi f_c & 0\\
0 & 0 & \frac{-\pi\alpha_2}{\alpha_1} & \frac{\pi^2}{\alpha_1} & 0 & 0\\
0 & \frac{1}{4\alpha_1} & -2\pi f_c & 0 & 1 & 0\\
-\frac{1}{4\alpha_1\beta} & 0 & 0 & 0 & 0 & \frac{1}{\beta^2}
\end{bmatrix}. \tag{A12}$$

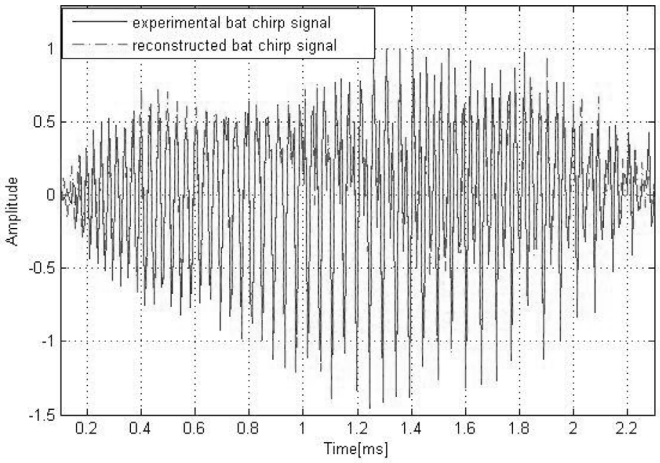

Fig. 7. Experimental bat chirp signal superimposed with the reconstructed signal.

The above matrix can be inverted analytically to obtain the inverse FIM:

$$I^{-1}(\Theta) = \frac{1}{f_s\zeta}\begin{bmatrix}
8\alpha_1^2 & 0 & 0 & 0 & 0 & 2\alpha_1\beta\\
0 & 8\alpha_1^2 & 0 & 0 & -2\alpha_1 & 0\\
0 & 0 & \frac{1}{\alpha_1} & \frac{\alpha_2}{\alpha_1\pi} & \frac{2\pi f_c}{\alpha_1} & 0\\
0 & 0 & \frac{\alpha_2}{\alpha_1\pi} & \frac{\alpha_1}{\pi^2} + \frac{\alpha_2^2}{\pi^2\alpha_1} & \frac{2\pi f_c\alpha_2}{\pi\alpha_1} & 0\\
0 & -2\alpha_1 & \frac{2\pi f_c}{\alpha_1} & \frac{2\pi f_c\alpha_2}{\alpha_1\pi} & \frac{3}{2} + \frac{(2\pi f_c)^2}{\alpha_1} & 0\\
2\alpha_1\beta & 0 & 0 & 0 & 0 & \frac{3\beta^2}{2}
\end{bmatrix}, \tag{A13}$$

where ζ denotes the SNR, i.e., $\zeta = (\beta^2 E/\sigma^2)$. The terms along the diagonal of the inverse FIM, $I^{-1}(\Theta)$, yield the CRLB on the variances of chirp model parameters:

$$\begin{aligned}
\mathrm{Var}\,(\hat{\alpha}_1) &\ge \frac{8\alpha_1^2}{f_s\zeta},\\
\mathrm{Var}\,(\hat{\alpha}_2) &\ge \frac{8\alpha_1^2}{f_s\zeta},\\
\mathrm{Var}\,(\hat{\tau}) &\ge \frac{1}{\alpha_1 f_s\zeta},\\
\mathrm{Var}\left(\hat{f}_c\right) &\ge \frac{\alpha_1^2+\alpha_2^2}{\pi^2\alpha_1 f_s\zeta},\\
\mathrm{Var}\left(\hat{\phi}\right) &\ge \frac{\frac{3}{2} + \frac{(2\pi f_c)^2}{\alpha_1}}{f_s\zeta},\\
\mathrm{Var}\left(\hat{\beta}\right) &\ge \frac{3\beta^2}{2f_s\zeta}.
\end{aligned} \tag{A14}$$

Acknowledgment

The authors wish to thank Curtis Condon, Ken White, and Al Feng of the Beckman Institute of the University of Illinois for the bat experimental data and for permission to use it in this paper.

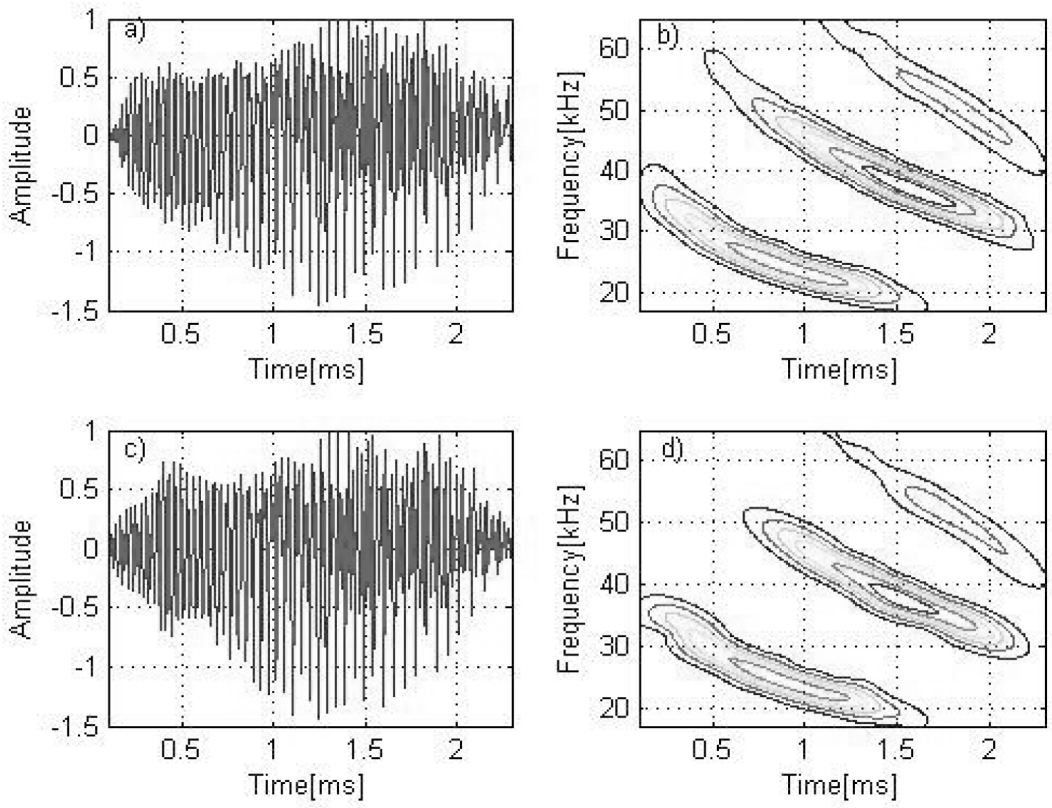

Fig. 8. (a) Experimental bat chirp signals. (b) CT of bat chirp signal in (a). (c) Reconstructed bat chirp signal. (d) CT of the reconstructed signal in (c).

References

[1] Y. Lu, G. Cardoso, R. Demirli, and J. Saniie, "Chirplet transform for ultrasonic signal analysis and NDE applications," in *Proc. IEEE Ultrason. Symp.*, Sep. 2005, pp. 536–539.

[2] J. Li and H. Ling, "Application of adaptive chirplet representation for ISAR feature extraction from targets with rotating parts," *IEE Proc. Radar, Sonar, Navigation*, vol. 150, pp. 284–291, Aug. 2003.

[3] G. Wang and X. Xia, "An adaptive filtering approach to chirp estimation and ISAR imaging of maneuvering targets," in *Proc. IEEE Int. Radar Conf.*, May 2000, pp. 481–486.

[4] W. Fan, H. Zou, Y. Sun, Z. Li, and R. Shi, "Decomposition of seismic signal via chirplet transform," in *Proc. IEEE 6th Int. Conf. Signal Processing*, Aug. 2002, pp. 1778–1782.

[5] N. Ma and D. Vray, "Bottom backscattering coefficient estimation from wideband chirp sonar echoes by chirp adapted time-frequency representation," in *Proc. IEEE Int. Conf., Acoust., Speech Signal Processing*, May 1998, pp. 12–15.

[6] G. Lopez-Risueno, J. Grajal, and O. A. Yeste-Ojeda, "CFAR detection of chirplets in coloured Gaussian noise," in *Proc. IEEE Conf., Acoust., Speech Signal Processing*, Apr. 2003, pp. 741–744.

[7] S. Krishnamachari and W. J. Williams, "Adaptive kernel design in the generalized marginal domain for time-frequency analysis," in *Proc. IEEE Int. Conf., Acoust., Speech, Signal Processing*, Apr. 1994, pp. 341–344.

[8] S. Mann and S. Haykin, "The chirplet transform: Physical considerations," *IEEE Trans. Signal Processing*, vol. 43, no. 11, pp. 2745–2761, Nov. 1995.

[9] S. Mann and S. Haykin, "Time-frequency perspectives: The chirplet transform," in *Proc. IEEE Int. Conf., Acoust., Speech Signal Processing*, Mar. 1992, pp. 417–420.

[10] S. Qian, D. Chen, and Q. Yin, "Adaptive chirplet based signal approximation," in *Proc. IEEE Int. Conf., Acoust., Speech, Signal Processing*, May 1998, pp. 1781–1784.

[11] A. Feng, X. Wu, and Q. Yin, "Fast algorithm of adaptive chirplet-based real signal decomposition," in *Proc. IEEE Int. Symp. Circuits Syst.*, Mar. 2001, pp. 6–9.

[12] X. Xia, "Discrete chirp-Fourier transform and its application to chirp rate estimation," *IEEE Trans. Signal Processing*, vol. 48, pp. 3122–3133, Nov. 2000.

[13] P. M. Djuric and S. M. Kay, "Parameter estimation of chirp signals," *IEEE Trans. Acoust. Speech Signal Processing*, vol. 38, pp. 2118–2126, Dec. 1990.

[14] G. Cardoso and J. Saniie, "Ultrasonic data compression via parameters estimation," *IEEE Trans. Ultrason., Ferroelect., Freq. Contr.*, vol. 52, pp. 313–325, Feb. 2005.

[15] G. Cardoso, "Compression, estimation, and analysis of ultrasonic signals," Ph.D. dissertation, Illinois Institute of Technology, Chicago, IL, May 2005.

[16] R. Demirli and J. Saniie, "Model-based estimation of ultrasonic echoes. Part I: Analysis and algorithms," *IEEE Trans. Ultrason., Ferroelect., Freq. Contr.*, vol. 48, pp. 787–802, May 2001.

[17] R. Demirli and J. Saniie, "Model-based estimation of ultrasonic echoes. Part II: Nondestructive evaluation applications," *IEEE Trans. Ultrason., Ferroelect., Freq. Contr.*, vol. 48, pp. 803–811, May 2001.

[18] R. Demirli and J. Saniie, "Model based time-frequency estimation of ultrasonic echoes for NDE applications," in *Proc. IEEE Ultrason. Symp.*, Oct. 2000, pp. 785–788.

[19] S. M. Kay, *Fundamentals of Statistical Signal Processing: Estimation Theory*. Englewood Cliffs, NJ: Prentice-Hall, 1998.

[20] C. Condon, K. White, and A. Feng, The bat data, Beckman Institute of the University of Illinois, Urbana, IL, http://www-dsp.rice.edu/software/bat.shtml.

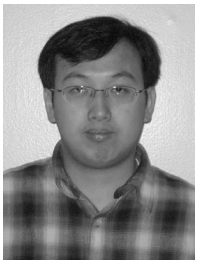

Yufeng Lu (S'06) was born in Jiangxi, China, on February 1, 1978. He received the B.Sc. degree in electrical engineering from Nanchang Institute of Aeronautics Technology, Nanchang, China, in 1998 and the M.S. degree in electrical engineering from Beijing University of Aeronautics and Astronautics in 2002. Since then, he has been studying for his Ph.D. degree in the area of communications and signal processing, the Department of Electrical and Computer Engineering, Illinois Institute of Technology, Chicago, IL.

His research interests include statistical signal processing, signal modeling, estimation and detection, embedded signal processors, and ultrasonic, nondestructive evaluation.

Ramazan Demirli was born in Isparta, Turkey, on November 11, 1970. He received the B.S. degree in electronics and communications engineering from the University of Uludag, Bursa, Turkey, in 1991. In 1993, he won a scholarship from the Turkish Ministry of Education to study abroad. He received his M.S. degree in electrical and computer engineering from the Illinois Institute of Technology (IIT), Chicago, IL, in 1995.

He received his Ph.D. degree in 2000 from the same department, specializing in statistical signal processing with extensive emphasis on ultrasonic signal processing and ultrasonic imaging. In particular, he has developed model-based estimation techniques for ultrasonic signal analysis and parameter estimation.

From 2000 to 2003 Dr. Demirli was with BrainMedia, LLC, New York, NY, where he assumed a major role in the development of a proprietary audio codec.

Dr. Demirli is currently with Canfield Scientific, Inc., Fairfield, NJ, where he conducts research for skin imaging systems and software development. He also serves as a postdoctoral research consultant to the Embedded Computing and Signal Processing (ECASP) Lab of IIT and provides guidance for ultrasonic signal processing research activities.

His current research interests are model-based signal analysis, superimposed signal estimation, and model-based image analysis. Dr. Demirli is a member of the IEEE.

Guilherme Cardoso was born in Porto Alegre, Brazil, on April 27, 1976. He received his B.S. degree in electrical engineering from the Federal University of Rio Grande do Sul, Brazil, and his M.S. and Ph.D. degrees in electrical and computer engineering from the Illinois Institute of Technology, Chicago, IL, in 1998, 2000, and 2005, respectively.

Dr. Cardoso has been at the Fermi National Accelerator Laboratory, Batavia, IL, since 1998, where he is the head of the Electronics Systems Engineering (ESE) Department. At ESE, he leads a group of over 30 engineers in the research, development, and production of electronics for tracking detectors and data acquisition systems used by high-energy particle physics, nuclear physics, and astrophysics experiments. Dr. Cardoso has had over 85 technical papers published.

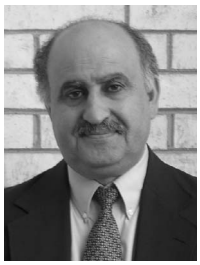

Jafar Saniie (S'80–M'81–M'83–SM'91) was born in Iran on March 21, 1952. He received his B.S. degree in electrical engineering from the University of Maryland in 1974. He received his M.S. degree in biomedical engineering in 1977 from Case Western Reserve University, Cleveland, OH, and his Ph.D. degree in electrical engineering in 1981 from Purdue University, West Lafayette, IN.

In 1981 Dr. Saniie joined the Department of Applied Physics, University of Helsinki, Finland, to conduct research in photothermal and photoacoustic imaging. Since 1983 he has been with the Department of Electrical and Computer Engineering at Illinois Institute of Technology where he is a professor, Director of the Ultrasonic Information Processing Laboratory, and Director of Graduate and Computer Engineering.

Dr. Saniie's research interests and activities are in ultrasonic signal and image processing, statistical pattern recognition, estimation and detection, embedded digital systems, digital signal processing with field programmable gate arrays, and ultrasonic nondestructive testing and imaging. In particular, he has performed extensive work in the areas of frequency diverse ultrasonic flaw enhancement techniques, embedded signal processing architectures for ultrasonic imaging, ultrasonic data compression, nonlinear signal processing in target detection, ultrasonic imaging of reverberant multilayer structures, morphological processing and pattern recognition in ultrasonic imaging, time-frequency analysis of ultrasonic signals, and applications of neural networks for detecting flaw echoes and classifying microstructural scattering. Dr. Saniie has been a technical committee member of the IEEE Ultrasonics Symposium since 1987 (currently he is the chair of Sensors, NDE and Industrial Applications), Associate Editor of the *IEEE Transactions on Ultrasonics, Ferroelectrics, and Frequency Control* since 1994, Program Coordinator and Local Chair of the Conference on Properties and Applications of Magnetic Materials since 1985, and Editorial Advisory member of the *Nondestructive Testing and Evaluation Journal* (1986–1996). He is a member of Sigma Xi, IEEE, Tau Beta Pi, Eta Kappa Nu, and he has been the IEEE Branch Counselor (1983–1990). He is the 1986 recipient of the Outstanding IEEE Student Counselor Award. He is the recipient of 2005 Outstanding Faculty Award in recognition of his excellence in teaching.